

# Jamming below upper critical dimension

Harukuni Ikeda<sup>1,\*</sup>

<sup>1</sup>*Laboratoire de Physique de l'École Normale Supérieure, ENS, Université PSL,  
CNRS, Sorbonne Université, Université de Paris, F-75005 Paris, France*

(Dated: June 6, 2022)

Extensive numerical simulations in the past decades proved that the critical exponents of the jamming of frictionless spherical particles remain unchanged in two and three dimensions. This implies that the upper critical dimension is  $d_u = 2$  or lower. In this work, we study the jamming transition below the upper critical dimension. We investigate a quasi-one-dimensional system: disks confined in a narrow channel. We show that the system is isostatic at the jamming transition point as in the case of standard jamming transition of the bulk systems in two and three dimensions. Nevertheless, the scaling of the excess contact number shows the linear scaling. Furthermore, the gap distribution remains finite even at the jamming transition point. These results are qualitatively different from those of the bulk systems in two and three dimensions.

PACS numbers: 64.70.Q-, 05.20.-y, 64.70.Pf

*Introduction.* – When compressed, particles interacting with finite ranged potential undergo the jamming transition at the critical packing fraction  $\varphi = \varphi_J$  at which particles start to touch, and the system acquires rigidity without showing apparent structural changes [1]. One of the most popular models of the jamming transition is a system consisting of frictionless spherical particles [2]. The nature of the jamming transition of the model is now well understood due to experimental and numerical investigations in the past decades [1]. A few remarkable properties are the following: (i) the system is nearly isostatic at  $\varphi_J$ ; namely, the number of constraints is just one greater than the number of degrees of freedom [3], (ii) the excess contact number  $\delta z$  from the isostatic value exhibits the power-law scaling  $\delta z \sim \delta\varphi^a$  where  $\delta\varphi = \varphi - \varphi_J$  denotes the excess packing fraction [2], (iii) the distribution of the gap between particles  $g(h)$  exhibits the power-law divergence  $g(h) \sim h^{-\gamma}$  at  $\varphi_J$  [4], and (iv) the critical exponents,  $a = 1/2$  and  $\gamma = 0.41$ , do not depend on the spatial dimensions  $d$  [2, 5].

On the theoretical side, one of the greatest achievements is the exact calculation of the critical exponents by using the mean-field models such as infinite dimensional hard spheres [5] and perceptron [6]. These models can be analyzed by using the notorious replica method, which was originally developed for polymers and spin-glasses [7]. The replica method predicts that systems undergo the replica symmetric breaking (RSB) transition before the jamming transition point [8]. Analyzing the jamming transition in the RSB phase, the replica theory can reproduce the isostaticity at  $\varphi_J$ , and the correct values of the critical exponents  $a$  and  $\gamma$  [5, 9]. These results imply that the upper critical dimension  $d_u$ , above which the mean-field theory provides correct results, is  $d_u \leq 2$ . Interestingly, an Imry-Ma-type argument [10] and recent finite size scaling analysis [11] also suggest  $d_u \leq 2$ .

A natural question is then what will happen below the upper critical dimension. To answer this question, we

here investigate the jamming transition for  $d < 2$ . However, the jammed configuration of a true  $d = 1$  system is trivial: for  $\varphi \geq \varphi_J$ , the number of contact per particle is just  $z = 2$ , unless next nearest neighbor particles begin to interact at very high  $\varphi$ . To obtain non-trivial results, we consider a quasi-one-dimensional system as shown in Fig. 1, where particles are confined between the walls at  $y = 0$  and  $y = L_y$ , and for  $x$ -direction, we impose the periodic boundary condition. In the thermodynamic limit with fixed  $L_y$ , the model can be considered as a one-dimensional system, but the jammed configuration is still far from trivial.

In the previous works, quasi-one-dimensional systems have been studied to elucidate the effect of confinement on the jamming transition [12, 13]. These studies uncover how the confinement changes the transition point  $\varphi_J$  [13] and the distribution of the stress near the walls [12]. However, the investigation of the critical properties is limited for the systems with very small  $L_y$  where the jammed configuration is similar to that of the true  $d = 1$  system: each particle contact with at most two particles, and therefore one can not discuss the scaling of  $\delta z$  [14–16]. To our knowledge, the scaling of  $\delta z$  for an intermediate value of  $L_y$  has not been studied before.

In this work, by means of extensive numerical simulations, we show that the system is always isostatic at the jamming transition point for all values of  $L_y$ , as in the case of the jamming in  $d \geq 2$ . Nevertheless, the critical behavior of the jamming of the quasi-one-dimensional system is dramatically different from the jamming transition in  $d \geq 2$ . We find that the excess contact number  $\delta z$ , and the excess constraints  $\delta c$ , which plays a similar role as  $\delta z$ , exhibit the linear scaling  $\delta z \sim \delta c \sim \delta\varphi$ . Furthermore, we find that  $g(h)$  remains finite even at  $\varphi_J$ . These results prove that the jamming transition of the quasi-one-dimensional system indeed shows the distinct scaling behaviors from those in  $d \geq 2$ .

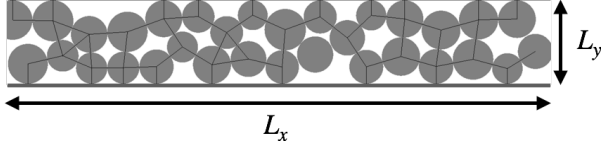


FIG. 1. A configuration at  $\varphi_J$  for  $N = 32$  and  $L_y = 2\sigma_{\max}$ . Gray circles represent particles, and the solid lines denote the contacts.

*Model.* – Here we describe the details of our model. We consider two dimensional disks in a  $L_x \times L_y$  box. For the  $y$ -direction, particles are confined between the walls at  $y = 0$  and  $y = L_y$ . For the  $x$ -direction, we impose the periodic boundary condition. The interaction potential of the model is given by

$$\begin{aligned}
 V_N &= \sum_{i < j}^{1,N} v(h_{ij}) + \sum_{i=1}^N v(h_i^b) + \sum_{i=1}^N v(h_i^t), \\
 h_{ij} &= |\mathbf{r}_i - \mathbf{r}_j| - \frac{\sigma_i + \sigma_j}{2}, \\
 h_i^b &= y_i - \frac{\sigma_i}{2}, \\
 h_i^t &= L_y - y_i - \frac{\sigma_i}{2}, \\
 v(h) &= k \frac{h^2}{2} \theta(-h).
 \end{aligned} \tag{1}$$

where  $\mathbf{r}_i = \{x_i, y_i\}$  and  $\sigma_i$  respectively denote the position and diameter of particle  $i$ ,  $h_{ij}$  denotes the gap function between particles  $i$  and  $j$ , and  $h_i^b$  and  $h_i^t$  respectively denote the gap functions between particle  $i$  and bottom and top walls. To avoid the crystallization, we consider polydisperse particles with uniform distribution  $\sigma_i \in [\sigma_{\min}, \sigma_{\max}]$ . Here after we set,  $k = 1$ ,  $\sigma_{\min} = 1$ , and  $\sigma_{\max} = 1.4$ .

*Numerics.* – We perform numerical simulations for  $N = 1024$  disks. We find  $\varphi_J$  by combining slow compression and decompression as follows [2]. We first generate a random initial configuration at a small packing fraction  $\varphi = 0.1$  between the walls at  $y = 0$  and  $y = L_y$ . Then, we slowly compress the system by performing an affine transformation along the  $x$ -direction. For each compression step, we increase the packing fraction with a small increment  $\delta\varphi = 10^{-3}$ , and successively minimize the energy with the FIRE algorithm [17] until the squared force acting on each particle becomes smaller than  $10^{-25}$ . After arriving at a jammed configuration with  $V_N/N > 10^{-16}$ , we change the sign and amplitude of the increment as  $\delta\varphi \rightarrow -\delta\varphi/2$ . Then, we decompress the system until we obtain an unjammed configuration with  $V_N/N < 10^{-16}$ . We repeat this process by changing the sign and amplitude of the increment as  $\delta\varphi \rightarrow -\delta\varphi/2$  every time the system crosses the jamming transition point. We terminate the simulation when  $V_N/N \in (10^{-16}, 2 \times 10^{-16})$ . We define  $\varphi_J$  as a packing fraction of this point.

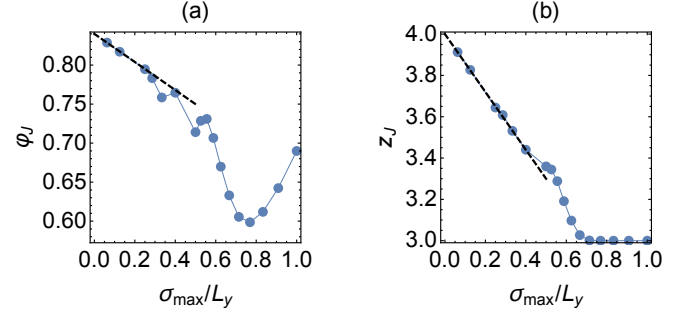


FIG. 2.  $L_y$  dependence of (a) the jamming transition point  $\varphi_J$  and (b) the contact number per particle at the jamming transition point  $z_J$ . Markers denote numerical results, and solid lines denote the guide to the eye. The dashed lines denote the linear fits  $\varphi_J = 0.84 - 0.28\sigma_{\max}/L_y$  and  $z_J = 4 - 1.4\sigma_{\max}/L_y$ .

After obtained a configuration at  $\varphi_J$ , we re-compress the system to obtain configurations above  $\varphi_J$ . As reported in Ref. [18], some fraction of samples become unstable during the compression (compression unjamming). We neglect these samples. We remove the rattlers that have less than three contacts before calculating physical quantities. Hereafter, we refer the number of the non-rattler particles as  $N_{\text{nr}}$ . To improve the statistics, we average over 50 independent samples.

$\varphi_J$  and  $z_J$ . – First, we discuss the  $L_y$  dependence of the jamming transition point  $\varphi_J$  and the contact number per particle at that point  $z_J$ . In Fig. 2 (a), we show  $\varphi_J$  as a function of  $\sigma_{\max}/L_y$ . For intermediate values of  $\sigma_{\max}/L_y$ ,  $\varphi_J$  shows a non-monotonic behavior. A similar non-monotonic behavior has been reported in a previous numerical simulation for a binary mixture [13]. In the limit  $\sigma_{\max}/L_y \rightarrow 0$ ,  $\varphi_J$  converges to its bulk value  $\varphi_J^{\text{bulk}} = 0.84$  as  $\varphi_J^{\text{bulk}} - \varphi_J \propto 1/L_y$ , see the dashed line in Fig. 2 (a). The same scaling has been observed in the previous simulation for the binary mixture [13]. The scaling implies the growing length scale

$$\xi \sim (\varphi_J^{\text{bulk}} - \varphi)^{-\nu} \tag{2}$$

with  $\nu = 1$ . It is worth mentioning that this is the same exponent observed by a correction to scaling analysis [19] and also our replica calculation for a confined system [20].

In Fig. 2 (b), we show  $z_J$  as a function of  $\sigma_{\max}/L_y$ . It is well known that  $z_J = z_J^{\text{bulk}} = 4$  for bulk two dimensional disks [2]. In the  $L_y \rightarrow \infty$  limit,  $z_J$  converges to the bulk value as  $z_J^{\text{bulk}} - z_J \sim 1/L_y$ , see the dashed line in Fig. 2 (b).

*Isostaticity.* – Next we discuss the isostaticity of the system. A system is referred to as isostatic when the number of constraints is the same as the number of degrees of freedom. For our system, the number of degrees of freedom of the non-rattler particles is  $N_f = 2N_{\text{nr}} - 1$

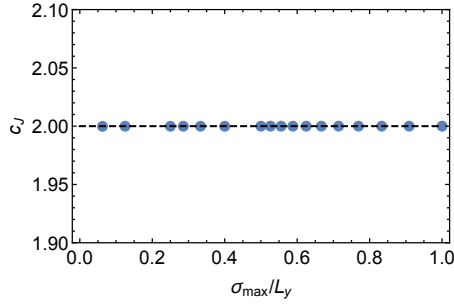


FIG. 3.  $L_y$  dependence of the number of constraints per particle at the jamming transition point  $c_J$ . Markers denote the numerical results, and the dashed line denotes the isostatic number  $c_{\text{iso}} = 2$ .

where we neglect the global translation along the  $x$ -axis. The number of constraints is

$$N_c = \frac{N_{\text{nr}}z - N_w}{2} + N_w = \frac{N_{\text{nr}}z}{2} + \frac{N_w}{2}, \quad (3)$$

where  $N_{\text{nr}}$  denotes the number of non-rattler particles,  $z$  denotes the number of contacts per particle,  $N_w$  denotes the number of contacts between particles and walls, and  $(N_{\text{nr}}z - N_w)/2$  accounts for the number of contacts between particles. When  $L_y \gg \sigma_{\text{max}}$ , the number of contacts between particles and walls can be negligible, and thus the isostatic condition  $N_c = N_f$  leads to  $z = 4$  in the thermodynamic limit. This condition is indeed satisfied in the case of the bulk  $d = 2$  system at  $\varphi_J$  [2]. On the contrary for  $L_y \sim \sigma_{\text{max}}$ , all particles may contact with walls  $N_w = N_{\text{nr}}$ , leading to  $z = 3$  for an isostatic system in thermodynamic limit. Fig. 2 (b) show that our model satisfies this condition at  $\varphi_J$  for  $\sigma_{\text{max}}/L_y \sim 1$ . To discuss the isostaticity for intermediate  $L_y$ , we introduce the number of constraints per particle  $c = N_c/N_{\text{nr}}$ . When the system is isostatic, we get  $c = c_{\text{iso}} = 2$  in the thermodynamic limit. In Fig. 3, we show our numerical result of  $c$  at  $\varphi_J$  as a function of  $\sigma_{\text{max}}/L_y$ . This plot proves that the system is always isostatic, irrespective of the value of  $L_y$ .

Now we shall discuss the behavior above  $\varphi_J$ . As mentioned in the introduction, we will investigate the model mainly for  $L_y > 2\sigma_{\text{min}}$  so that some fraction of disks can path through, and thus the contact network undergoes a non-trivial rearrangement on the change of  $\varphi$ .

*Energy and pressure.* – For  $\varphi > \varphi_J$ , the particles overlap each other. As a consequence, the energy  $V_N$  and pressure  $p$  have finite values. Since we only consider the compression along the  $x$ -axis, we define the pressure as

$$p = -\frac{1}{V} \left. \frac{\partial V_N(\{x'_i\})}{\partial \varepsilon} \right|_{\varepsilon=0} = -\frac{1}{V} \sum_{i < j} v'(h_{ij}) \frac{(x_i - x_j)^2}{|\mathbf{r}_i - \mathbf{r}_j|}, \quad (4)$$

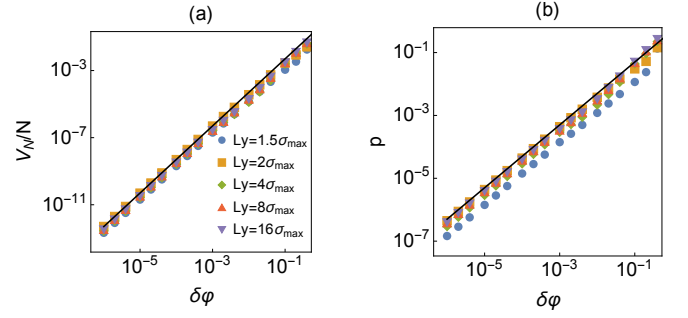


FIG. 4. (a)  $\delta\varphi$  dependence of the energy per particle  $V_N/N$ . Marker denote numerical results, and the solid line denotes  $\delta\varphi^2$ . (b)  $\delta\varphi$  dependence of the pressure  $p$ . Marker denote numerical results, and the solid line denotes  $\delta\varphi$ .

where  $V = L_x L_y$ , and  $x'_i = x_i(1 + \varepsilon)$  denotes the affine transformation along the  $x$ -axis. In Fig. 4, we show the  $\delta\varphi$  dependence of  $V_N/N$  and  $p$ . We find the scalings  $V_N/N \sim \delta\varphi^2$  and  $p \sim \delta\varphi$ . The same scalings were observed for the bulk systems in  $d = 2$  and  $d = 3$  [2].

*Number of constraints and contacts.* – Next we observe the density dependence of the number of constraints. For this purpose, we introduce the excess constraints as

$$\delta c = \frac{N_c - N_f - 1}{N_{\text{nr}}}. \quad (5)$$

where  $N_f + 1$  denotes the minimal number of constraints to stabilize a system [21]. For the bulk limit  $L_y \sim \sigma_{\text{max}}\sqrt{N}$ ,  $\delta c$  can be identified with the excess contact number  $\delta z$ . In this case, the extensive finite size scaling analysis proved the following scaling form [21]:

$$\delta c = N^{-1} \mathcal{C}(N^2 \delta\varphi), \quad (6)$$

where the scaling function  $\mathcal{C}(x)$  behaves as

$$\mathcal{C}(x) \sim \begin{cases} x^{1/2} & x \gg 1 \\ x & x \ll 1. \end{cases} \quad (7)$$

This implies that the square root behavior  $\delta c \sim \delta\varphi^{1/2}$  is truncated at  $\delta\varphi \sim N^{-2}$  for a finite  $N$  system. For  $\delta\varphi \ll N^{-2}$ , one observes a linear scaling behavior  $\delta c \sim N\delta\varphi$  [19].

To investigate how the behavior changes for  $L_y \ll \sigma_{\text{max}}\sqrt{N}$ , in Fig. 5 (a), we show the  $\delta\varphi$  dependence of  $\delta c$  for several  $L_y$ . For large  $L_y$  and intermediate  $\delta\varphi$ , we observe the square root scaling  $\delta c \sim \delta\varphi^{1/2}$ . On the contrary, for small  $L_y$  and small  $\delta\varphi$ ,  $\delta c$  shows the linear behavior  $\delta c \sim \delta\varphi$ . To discuss the scaling behavior more closely, we assume the following scaling form:

$$\delta c = l_y^\alpha \mathcal{C}'(l_y^\beta \delta\varphi), \quad (8)$$

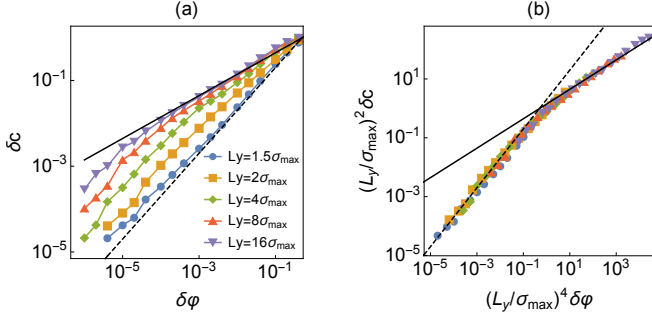


FIG. 5. (a)  $\delta c$  as a function of  $\delta\varphi$ . Markers denote numerical results. The solid and dashed lines denote  $\delta c \sim \delta\varphi^{1/2}$  and  $\delta c \sim \delta\varphi$ , respectively. (b) Scaling plot for the same data.

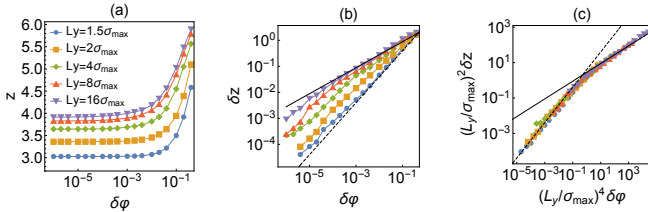


FIG. 6. (a)  $z$  as a function of  $\delta\varphi$ . Markers denote numerical results. (b)  $\delta z = z - z_J$  as a function of  $\delta\varphi$ . The solid and dashed lines denote  $\delta z \sim \delta\varphi^{1/2}$  and  $\delta z \sim \delta\varphi$ , respectively. (c) Scaling plot for the same data.

where  $l_y = L_y/\sigma_{\max}$ , and  $\mathcal{C}'(x)$  shows the same scaling behavior as  $\mathcal{C}(x)$ , Eq. (7). When  $l_y \sim \sqrt{N}$ , the scaling should converge to that of the bulk  $d = 2$  system, Eq. (6). This requires  $\alpha = -2$  and  $\beta = 4$ . In Fig. 5, we test this prediction. A good scaling collapse verifies the scaling function Eq. (8).

Note that for a bulk system in  $d \geq 2$ , the system exhibits the linear scaling only for  $\delta\varphi \ll N^{-2}$ ; the linear regime vanishes in the thermodynamic limit. Contrary, Eq. (8) implies that the linear scaling regime persists even in the thermodynamic limit for the quasi-one-dimensional system as long as  $L_y$  is finite. Therefore, the quasi-one-dimensional system indeed has a distinct critical exponent from that of the bulk systems in  $d \geq 2$ .

In Figs.(a)–(c), we also show the behaviors of the contact number per particle  $z$ , excess contacts  $\delta z = z - z_J$ , and its scaling plot. The data for  $\delta z$  is more noisy than  $\delta c$ , presumably due to the fluctuation of  $z_J$ , but still we find a reasonable scaling collapse by using the same scaling form as  $\delta c$ .

*Gap distribution.* – Another important quantity to characterize the critical property of the jamming transition is the gap distribution  $g(h)$ . For the bulk systems in  $d \geq 2$ ,  $g(h)$  exhibits the power-law divergence at  $\varphi_J$ :

$$g(h) \sim h^{-\gamma} \quad (9)$$

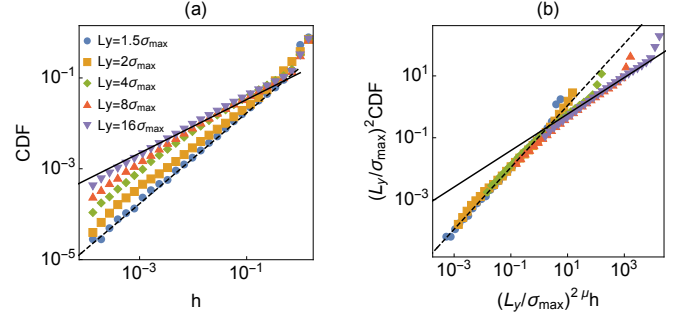


FIG. 7. (a) CDF of the gap function  $h$ . Markers denote numerical results. The solid and dashed lines denote  $h^{1-\gamma}$  and  $h^1$ , respectively. (b) Scaling plot for the same data.

with  $\gamma = 0.41$  [5]. In order to improve the statistics, we observe the cumulative distribution function (CDF) of the gap functions ( $h_{ij}$  and  $h_i^{t,b}$ ), instead of  $g(h)$  itself. In this case, the power-law divergence Eq. (9) appears as  $\text{CDF} \sim h^{1-\gamma}$ . In Fig. 7 (a), we show our numerical results of CDF for several  $L_y$ . We find that for small  $L_y$  and  $h$ ,  $\text{CDF} \sim h$  meaning that  $g(h)$  remains finite  $g(h) \sim h^0$  even at  $\varphi_J$ . On the contrary, for large  $L_y$ , there appears the intermediate regime where  $\text{CDF} \sim h^{1-\gamma}$ , as in  $d \geq 2$ . To discuss the crossover from  $\text{CDF} \sim h$  to  $\text{CDF} \sim h^{1-\gamma}$ , we assume the following scaling form:

$$\text{CDF} = l_y^\zeta \mathcal{F}'(l_y^\eta h), \quad (10)$$

where the scaling function  $\mathcal{F}'(x)$  behaves as

$$\mathcal{F}'(x) \sim \begin{cases} x^{1-\gamma} & x \gg 1 \\ x & x \ll 1. \end{cases} \quad (11)$$

When  $l_y \sim \sqrt{N}$ , this should converge to the scaling form for finite  $N$ ,  $\text{CDF}(h) = N^{-1} \mathcal{F}(N^\mu h)$ , where  $\mu = 1/(1-\gamma)$ , and  $\mathcal{F}(x)$  shows the same scaling as Eq. (11) [22]. This requires  $\zeta = -2$  and  $\eta = 2\mu$ . In Fig. 7 (b), we check this prediction. The excellent collapse proves the validity of our scaling Ansatz Eq. (10).

*Conclusions.* – In this work, we showed that the jamming transition in a quasi-one-dimensional system is qualitatively different from that in  $d \geq 2$  systems: the excess constraints and contacts exhibit the linear scaling  $\delta c \sim \delta z \sim \delta\varphi$ , instead of the square root scaling  $\delta z \sim \delta\varphi^{1/2}$ , and the gap distribution  $g(h)$  remains finite even at  $\varphi_J$ , instead of the power-law divergence  $g(h) \sim h^{-\gamma}$ .

Important future work is to test the robustness of our results for other shapes of the quasi-one-dimensional geometries such as a  $d$ -dimensional box with a fixed length in the  $d - 1$  directions and an infinite length in only one direction, and circular cylinder with a fixed radius.

Interestingly, the same scaling behavior of that of our model has been reported for a model of random linear

programming [6], where the system becomes isostatic at the jamming transition point, but the RSB does not happen. As a consequence,  $g(h)$  remains finite and regular. Considering this result, our results may imply that the RSB phase does not appear even at  $\varphi_J$  in  $d = 1$ , while it does in  $d = 2$ , namely, the lower critical dimension of the RSB at  $\varphi_J$  is  $1 < d_l < 2$ . Further theoretical, numerical, and experimental investigations are necessary to elucidate this point [23–26].

*Acknowledgements.* – We warmly thank M. Ozawa, A. Ikeda, K. Hukushima, Y. Nishikawa, F. Zamponi, P. Urbani, and M. Moore for discussions related to this work. This project has received funding from the European Research Council (ERC) under the European Union’s Horizon 2020 research and innovation program (grant agreement n. 723955-GlassUniversality).

---

\* harukuni.ikeda@ens.fr

- [1] A. J. Liu and S. R. Nagel, *Annu. Rev. Condens. Matter Phys.* **1**, 347 (2010).
- [2] C. S. O’Hern, L. E. Silbert, A. J. Liu, and S. R. Nagel, *Phys. Rev. E* **68**, 011306 (2003).
- [3] J. Bernal and J. Mason, *Nature* **188**, 910 (1960).
- [4] A. Donev, S. Torquato, and F. H. Stillinger, *Phys. Rev. E* **71**, 011105 (2005).
- [5] P. Charbonneau, J. Kurchan, G. Parisi, P. Urbani, and F. Zamponi, *Nat. Commun.* **5**, 3725 (2014).
- [6] S. Franz and G. Parisi, *Journal of Physics A: Mathematical and Theoretical* **49**, 145001 (2016).
- [7] M. Mézard, G. Parisi, and M. Virasoro, *Spin glass theory and beyond: An Introduction to the Replica Method and Its Applications*, Vol. 9 (World Scientific Publishing Company, 1987).
- [8] J. Kurchan, G. Parisi, P. Urbani, and F. Zamponi, *The Journal of Physical Chemistry B* **117**, 12979 (2013).
- [9] S. Franz, G. Parisi, M. Sevelev, P. Urbani, and F. Zamponi, *SciPost Phys* **2**, 019 (2017).
- [10] M. Wyart, *arXiv preprint cond-mat/0512155* (2005).
- [11] D. Hexner, P. Urbani, and F. Zamponi, *Phys. Rev. Lett.* **123**, 068003 (2019).
- [12] J. W. Landry, G. S. Grest, L. E. Silbert, and S. J. Plimpton, *Physical review E* **67**, 041303 (2003).
- [13] K. W. Desmond and E. R. Weeks, *Phys. Rev. E* **80**, 051305 (2009).
- [14] S. S. Ashwin and R. K. Bowles, *Phys. Rev. Lett.* **102**, 235701 (2009).
- [15] S. S. Ashwin, M. Zaeifi Yamchi, and R. K. Bowles, *Phys. Rev. Lett.* **110**, 145701 (2013).
- [16] M. J. Godfrey and M. A. Moore, *Phys. Rev. E* **89**, 032111 (2014).
- [17] E. Bitzek, P. Koskinen, F. Gähler, M. Moseler, and P. Gumbsch, *Phys. Rev. Lett.* **97**, 170201 (2006).
- [18] K. VanderWerf, A. Boromand, M. D. Shattuck, and C. S. O’Hern, *Phys. Rev. Lett.* **124**, 038004 (2020).
- [19] D. Vågberg, D. Valdez-Balderas, M. A. Moore, P. Olsson, and S. Teitel, *Phys. Rev. E* **83**, 030303 (2011).
- [20] H. Ikeda and A. Ikeda, *EPL (Europhysics Letters)* **111**, 40007 (2015).
- [21] C. P. Goodrich, A. J. Liu, and S. R. Nagel, *Physical review letters* **109**, 095704 (2012).
- [22] H. Ikeda, C. Brito, and M. Wyart, *arXiv preprint arXiv:1908.02091* (2019).
- [23] P. Urbani and G. Biroli, *Phys. Rev. B* **91**, 100202 (2015).
- [24] A. Seguin and O. Dauchot, *Phys. Rev. Lett.* **117**, 228001 (2016).
- [25] P. Charbonneau and S. Yaida, *Physical review letters* **118**, 215701 (2017).
- [26] C. L. Hicks, M. J. Wheatley, M. J. Godfrey, and M. A. Moore, *Phys. Rev. Lett.* **120**, 225501 (2018).